



Research Paper

Paper No.: 2023-JL-03  
Online: ISSN: 2583-3707

**ARAI Journal of Mobility Technology**  
<https://araijournal.com/index.php/arai>  
Volume 3 • Issue 4 • October – December, 2023, pp.788-802  
DOI:10.37285/ajmt.3.4.3

---

# Predicting base Engine Vibrations using Flexible Multi Body Dynamics Simulation

---

## Author's Affiliations

**Pranay Sharma, Nikhil Rao, Rentong Wang and Pravin Kakde**  
Cummins Technical Center India, Cummins Inc.

**\*Corresponding Author: Mr. Pranay Sharma**, Cummins Technical Center India,  
Cummins Inc., Gandhi Bhavan Rd, Dahanukar Colony, Kothrud, Pune,  
Maharashtra 411038

**Email:** pranay.sharma@cummins.com

## Article History

Received 27/07/2023

Accepted 25/04/2023

Published 15/12/2023

Copyright © ARAI, Pune

## Keywords

Engine dynamics, Model fidelity, Sub-structuring, Engine rolling, twisting, and bending, Engine major orders, Peak-hold spectrum analysis

---

**Cite this paper as:** Pranay Sharma, Nikhil Rao, Rentong Wang and Pravin Kakde (2023) "Predicting base Engine Vibrations using Flexible Multi Body Dynamics Simulation, ARAI Journal of Mobility Technology, 3(4), pp. 788-802.

Available at: <https://doi.org/10.37285/ajmt.3.4.3>

---

## Abstract

Predicting the vibratory response of a base engine is appealing as it can speed up the engine development cycle and cut down testing cost. However, there are concerns regarding predictability of base engine vibration simulation models due to various factors. This study attempts to investigate this predictability and gives more insights on what factors can affect it. In the presented work, the vibratory response of a base engine is predicted through a flexible Multi Body Dynamics simulation. Cylinder pressure excitation on the cylinder head and pistons, and reciprocating inertia excitation, are considered as inputs in this flexible Multi Body Dynamics simulation. Effects arising from overhead moving components and gear train, have been excluded from this study. The predicted vibratory response of the base engine at particular locations, is compared with the vibratory response as measured using accelerometers mounted at those locations, during testing. A reasonable level of correlation can be seen between simulation and testing. Measures that can be taken to improve this correlation are also discussed.

## Introduction

There are several attachments on the base engine, each playing a crucial role in the working of an engine. Some of these attachments are intake and exhaust manifolds, fuel and lube filters, oil pan, and Electronic Control Module. Evaluating the structural integrity of attachments is integral to the development of a new engine.

A harmonic response analysis<sup>[1]</sup> of an attachment design helps in evaluating the attachment's structural integrity early in the engine development process. Performing this analysis requires the availability of the input vibratory excitation provided to the attachment by the base engine. However, since the engine development process is still in an early phase, this input vibratory excitation usually cannot be measured.

This compels the harmonic response analysts to estimate the input vibratory excitation based on historically available data, which can, at times, lead to the attachment being under-designed, and hence failing during the subsequent engine testing. This estimation of input vibratory excitation based on historically available data can, at other times, also lead to the attachment being over-designed, and hence not being cost-effective. Through the work that is being presented in this paper, it is being investigated whether simulation can help in overcoming this reliance on historically available data.

The key question that is being answered is that, if a simulation of the engine is performed using the same inputs as that in a test cell, then, how accurately can the base engine vibration be predicted. To answer this key question, an inline six-cylinder engine is used as an example, in the presented work.

The structure of the paper is as follows. The next section describes the steps followed to model the engine. On performing simulation using this model, vibration of the base engine is predicted, which is postprocessed using three techniques. These three techniques are described in the 'Postprocessing' section. The same postprocessing is also carried out on measured base engine vibration data. In the 'Results' section, the postprocessed predicted vibration data and the postprocessed measured vibration data are compared to each other, using charts. The 'Discussion' section has a discussion on the charts shown in the 'Results' section. Finally, the conclusion of the work and the next steps are discussed in the 'Conclusions' section.

## Modeling of the Engine

The modeling of the engine to predict the base engine vibrations can broadly be divided into three steps. These steps are:

- 1 Finite Element (FE) Modeling of the stationary parts of the engine

- 2 Sub-structuring of the Finite Element Model
- 3 Three-Dimensional (3D) flexible Multi Body Dynamic (MBD) simulation of the complete engine

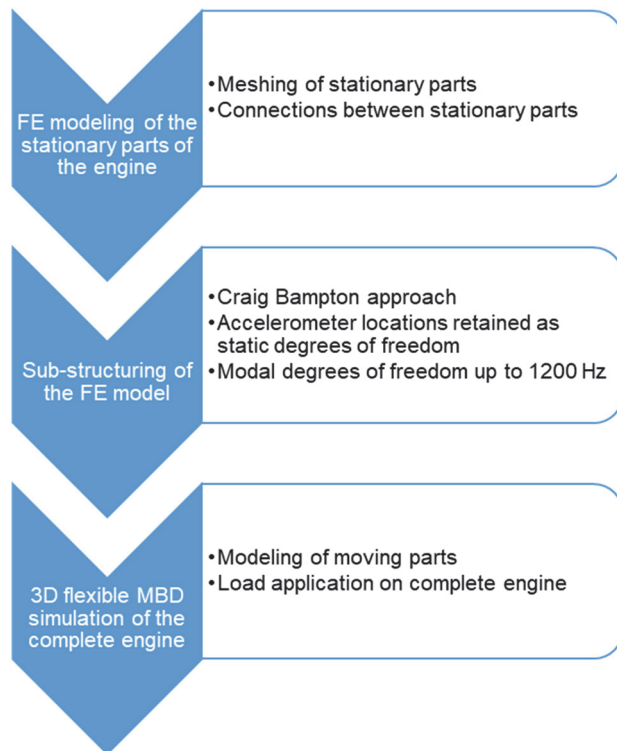


**Figure 1.** Steps in engine modeling.

### Finite Element Modeling of the stationary parts of the engine

A three-dimensional model of the assembly of all stationary parts of the engine, is prepared and imported into a Finite Element Analysis software, where they are meshed using quadratic elements.

Ultimately, a comparison between the vibratory response as recorded by the accelerometers on the base engine, and that predicted by simulation is to be made. Therefore, at this stage, care should be taken that there are mesh nodes exactly at the accelerometer locations on the base engine. This is important because later, the degrees of freedom of these mesh nodes will be retained as static degrees of freedom, during sub-structuring of this Finite Element Model.

Further, connections need to be established between mating parts in the Finite Element Model.

In the work that is discussed in this paper, the software used for Finite Element Modeling of the

stationary parts of the engine, is ANSYS Mechanical.

### Sub-structuring of the Finite Element Model

The Finite Element Model of the stationary parts of the engine, has been built in the previous step, with the intention of coupling it with the models of moving parts of the engine, to result in the model of the complete engine. However, the complete engine model, can become computationally expensive to simulate, if the Finite Element Model is used, as is.

Sub-structuring<sup>[2]</sup> of the Finite Element Model is, therefore, often necessary. Using super-elements is an efficient method of sub-structuring. A super-element can be formed either using static reduction or dynamic reduction. However, since the dynamic response of the Finite Element Model is important in answering this work's key question, dynamic reduction is chosen. Among the dynamic reduction techniques, the Craig Bampton type of dynamic reduction<sup>[3]</sup>, is chosen, in which the super-element retains information from both static degrees of freedom and modal degrees of freedom.

As mentioned earlier, the degrees of freedom of the mesh nodes at the accelerometer locations, are retained as static degrees of freedom.

The modal degrees of freedom come after performing a modal analysis of the Finite Element Model with all the static degrees of freedom constrained in space. The modal analysis is run for natural frequencies up to 1200 Hz.

### Three Dimensional flexible Multi Body Dynamic simulation of the complete engine

In the previous two steps, the Finite Element Model of the stationary parts of the engine was built and dynamically condensed. In this step, the model of the complete engine, including the moving parts, is built, assembled, and simulated. In the current work, the software used for this purpose is AVL Excite Powerunit.

The moving parts of the engine, that may play a key role in the base engine vibration, like the crankshaft, piston, and connecting rod are modeled.

Connections are then, established between the condensed stationary parts and the moving parts. These connections may vary, in complexity, from a perfectly revolute joint with no angular misalignment between the journal and the bearing, to an Elasto-Hydro-Dynamic joint, that considers not just this angular misalignment, but also compliance of the bearing support.

Further, connections are established between the condensed stationary model and the ground. These connections may be modeled through a low or a high joint stiffness, depending on whether, these connections are having vibration isolators or not.

This completes modeling of the complete engine. The next step is to apply external loads on this complete engine model.

There are three external loads that are considered.

- 1 Upward force on the fire deck of the cylinder head from combustion in the cylinders
- 2 Downward force on the pistons because from combustion in the cylinders
- 3 Brake torque on the flywheel from the test cell dynamometer

Application of these external loads makes the complete engine model ready for simulation.

### Uncertainty in inputs

While performing engine modeling described by steps 2.1 to 2.3, it was attempted to use inputs that are best representative of the test cell scenario. Among all the modeling inputs, there are three in which, the likelihood of deviation from the test cell scenario, is higher than others. These are:

- 1 Instantaneous pressure in the cylinders
- 2 Modeling of the rotating assembly that is attached to the rear of the flywheel
- 3 Stiffness of the vibration isolators that are used to connect the condensed stationary model to the ground

The cause of uncertainty in these inputs is described below:

### Instantaneous pressure in the cylinders

The instantaneous pressure in the cylinders determines all the three external loads on the engine model, namely, the upward force on the fire deck of the cylinder head, the downward force on the pistons, and the brake torque on the flywheel from the test cell dynamometer.

As this instantaneous pressure in the cylinders was not measured in the test cell simultaneously with the vibration measurement, it was decided to use an instantaneous pressure data that was available in a database, and was recorded earlier, for a similar engine performance.

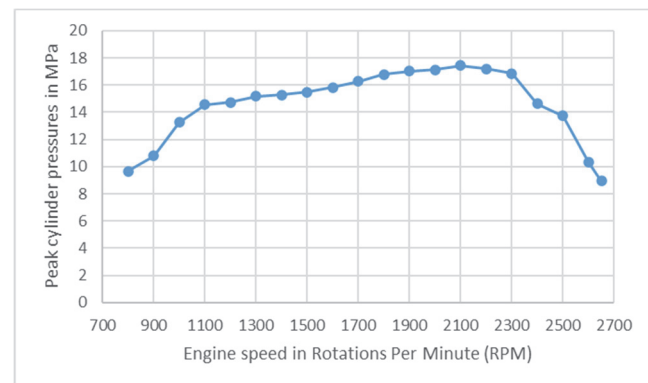


**Figure 2.** Peak cylinder pressures in the available data.

### Modeling of the rotating assembly that is attached to the rear of the flywheel

The inertia and stiffness of the rotating assembly that is attached to the rear of the flywheel, impact the torsional<sup>[4,5]</sup> and bending<sup>[6]</sup> response of the crankshaft assembly. The bending response of the crankshaft may affect the local deformation of the cylinder block as well because the crankshaft and cylinder block are connected through main bearings.

Due to some constraints, accurate information about the rotating assembly that is attached to the rear of the flywheel, in the test cell where the base engine vibration was measured, was not available. Therefore, estimation based on previous torsional vibration tests in the same test cell, was used to model this rotating assembly.

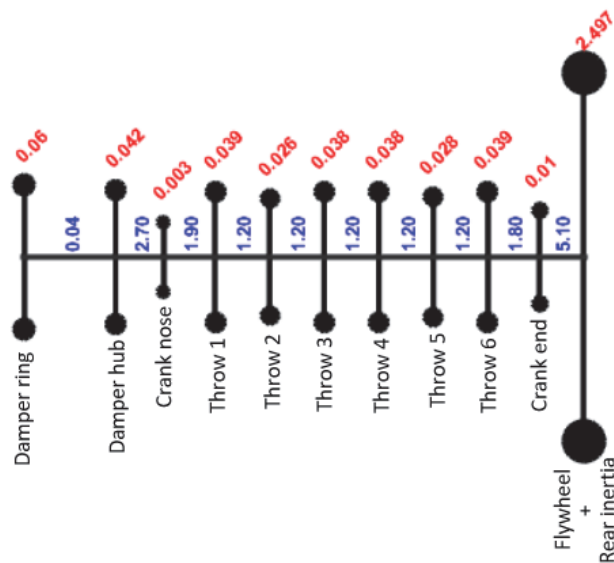


**Figure 3.** Torsional characteristics of the rotating assembly (red values are inertias in  $\text{kgm}^2$  and blue values are stiffnesses in  $10^6 \text{ Nm/rad}$ ).

### Stiffness of the vibration isolators that are used to connect the condensed stationary model to the ground

The supplier of the vibration isolators provided a static stiffness value of  $4e5 \text{ N/m}$ . It is known that vibration isolator materials like rubber offer a higher stiffness under dynamic loading as compared to static loading<sup>[7]</sup>. So, a multiplier of 1.4 was used on the supplier-provided static stiffness, to compute the dynamic stiffness of vibration isolators. This multiplier was based on previous experience and may bring in some uncertainty with it.

Further, the static stiffness value provided by the supplier, was for only one direction of loading on the vibration isolator (which aligned to the engine vertical direction). Therefore, the stiffness along the other directions had to be estimated based on the geometry of the vibration isolator. Thus, the stiffness along the engine lateral direction was considered to be the same as that in the engine vertical direction, and the stiffness along the engine axial direction was assigned a significantly high value of  $1e8 \text{ N/m}$  as an attempt to model a near-rigid axial geometry.

## Postprocessing

After the simulation run for all engine speeds from low to high idle conditions, is complete, the predicted vibration data is postprocessed in three ways, that are described in sections 3.1, 3.2, and 3.3. Similar postprocessing is also carried out on the measured vibration data. Since, two out of these three postprocessing ways are order based, a short discussion on ‘order’ is given here.

Using Fourier transformation<sup>[8,9]</sup>, a time varying signal can be decomposed into multiple harmonic components, each having a different frequency, amplitude, and phase. From an engine’s perspective, a signal’s harmonic component has an order equal to  $N$ , if its frequency is  $N$  times the frequency of crankshaft rotation. For example, if the engine speed is 1200 RPM, then the frequency of crankshaft rotation is 20 Hz, and any signal’s harmonic component having a frequency of 90 Hz, is said to have an order of 4.5.

Currently, the engine being considered is an inline six-cylinder engine, with an equally spaced firing sequence<sup>[10]</sup> of 1-5-3-6-2-4. Because of this, at any engine speed, when the excitation on the crankshaft, from the cylinder pressure and reciprocating inertia loads<sup>[11]</sup>, is decomposed using Fourier transformation, it results in four specific harmonic components, having an excitation amplitude, much higher than that of other harmonic components. These specific harmonic components have orders of 1.5, 3, 4.5, and 6, and these components are said to be ‘major order’ components. Consequently, at any engine speed, the vibratory response too, corresponding to these major order harmonic components is higher, compared to other harmonic components.

An explanation of the three postprocessing methods, used for both predicted and measured vibration data, follows.

### Peak-hold acceleration magnitude versus frequency

This postprocessing technique is carried out on three locations on the cylinder head. These three locations are marked with numbers 1 to 3, in the figure below.

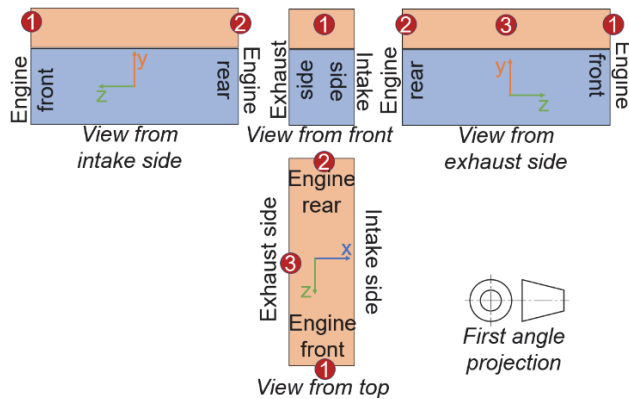


**Figure 4.** Locations of accelerometers 1 to 3 on the base engine.

The first location is on the front face of cylinder head. The second location is on the rear face of cylinder head. The third location is on the exhaust face of cylinder head and may be considered as the location of input vibratory excitation, for the exhaust manifold.

For any location, at any engine speed, the acceleration versus time data is resolved into three Cartesian directions, namely, x, y, and z, which are as shown in the figure 2. By performing Fourier transformation on each of the three directional accelerations, their magnitude versus frequency information, is obtained.

This exercise is repeated for all the engine speeds. So, now, for example, each frequency has multiple lateral (x direction as shown in figure 2) acceleration magnitudes, each lateral acceleration magnitude corresponding to a different engine speed. The envelope of maximum lateral acceleration magnitudes is plotted against frequency. This is done for the other two directions, that is, vertical and axial directions (y and z directions, respectively, as shown in figure 2), as well.

Results obtained by this postprocessing method using both predicted and measured vibration data, are shown in the 'Results: Peak-hold acceleration magnitude versus frequency' section.

### Order-wise acceleration magnitude versus engine speed

This postprocessing technique is carried out on only the third location on the cylinder head.

At any engine speed, again, the acceleration versus time data, is used as an input for postprocessing. Again, this data is resolved into the three Cartesian directions. By performing Fourier transformation on each of the three directional accelerations, their magnitude versus order information, is obtained.

This exercise is repeated for each engine speed, and so, the directional acceleration magnitude for each major order, is plotted against engine speed.

Results obtained by this postprocessing method using both predicted and measured vibration data, are shown in the 'Results: Order-wise acceleration magnitude versus engine speed' section.

### Order-wise base engine roll, twist, and bend magnitude versus engine speed

Five locations on the pan-rail, are needed to carry out this postprocessing technique. These five locations are marked with numbers 4 to 8, in figure 3.

The fourth, fifth, and sixth locations are on the intake side pan-rail. The seventh and eighth locations are on the exhaust side pan-rail. The fourth and seventh locations are close to the front of the engine. The fifth location is close to the middle of the engine. The sixth and eighth locations are close to the rear of the engine.

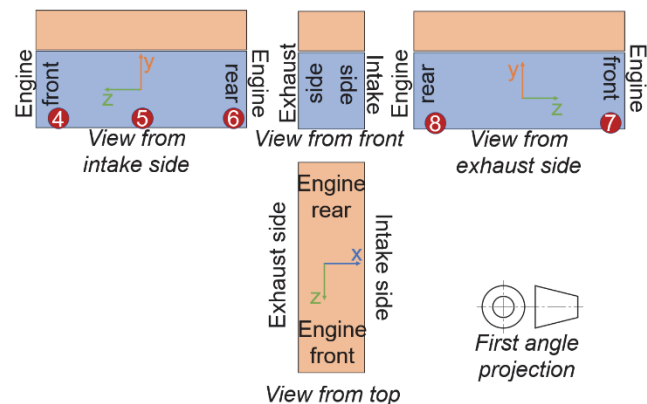


**Figure 5.** Locations of accelerometers 4 to 8 on the base engine.

This postprocessing method is similar to the ones described in sections 3.1 and 3.2, till the step of performing Fourier transformation on each of the three directional accelerations. Through this Fourier transformation, directional acceleration magnitude versus order information, and directional acceleration phase versus order information are obtained.

Then, assuming simple harmonic motion, this data is converted into directional displacement magnitude versus order information and directional displacement phase versus order information.

Using the magnitude and phase information, the time varying displacement for any order can be obtained. Mathematical operations are performed on these order-wise time varying displacements of multiple locations, to obtain information about how much the base engine is rolling, twisting, and bending, at each order.

These mathematical operations are as given below.

#### For computing the base engine roll metric

$$\theta_{roll} = \text{average}(\theta_{front}, \theta_{rear}) \quad \dots(1)$$

$$\theta_{front} = \sin^{-1}(y_4 - y_7) / d_{47} \quad \dots(2)$$

$$\theta_{rear} = \sin^{-1}(y_6 - y_8) / d_{68} \quad \dots(3)$$

$\theta_{roll}$  is the base engine roll metric.  $\theta_{front}$  is the angular deflection at the front of the engine.  $\theta_{rear}$  is the angular deflection at the rear of the engine.  $d_{47}$  and  $d_{68}$  are distances between the fourth and seventh locations, and the sixth and eighth locations, respectively.

For any order,  $y_4$ ,  $y_7$ ,  $y_6$ , and  $y_8$  are time varying displacements in the engine vertical direction (y direction as shown in figure 3), at the fourth, seventh, sixth, and eighth locations, respectively. Therefore,  $\theta_{front}$  and  $\theta_{rear}$  are also varying with time. Consequently, the average of these two quantities,  $\theta_{roll}$ , is also varying with time. The maximum value obtained by  $\theta_{roll}$ , for major orders, is noted.

This exercise is repeated for all the engine speeds. The maximum value obtained by  $\theta_{roll}$ , for major orders, is thus, plotted against the engine speeds.

#### For computing the base engine twist metric

$$\theta_{twist} = \theta_{front} - \theta_{rear} \quad \dots(4)$$

$\theta_{twist}$  is the base engine twist metric. The definitions of  $\theta_{front}$  and  $\theta_{rear}$  are the same as in the case of base engine roll metric. Also, just like  $\theta_{roll}$ ,  $\theta_{twist}$  is also varying with time. The maximum value obtained by  $\theta_{twist}$ , for major orders, is noted.

This exercise is repeated for all the engine speeds. The maximum value obtained by  $\theta_{twist}$ , for major orders, is thus, plotted against the engine speeds.

#### For computing the base engine bend metric

$$b = \text{average}(x_4, x_6) - x_5 \quad \dots(5)$$

$b$  is the base engine bend metric. For any order,  $x_4$ ,  $x_6$ , and  $x_5$  are time varying displacements in the engine lateral direction (x direction as shown in figure 3), at the fourth, sixth, and fifth locations, respectively. Therefore,  $b$  is also varying with time. The maximum value obtained by  $b$ , for major orders, is noted.

This exercise is repeated for all the engine speeds. The maximum value obtained by  $b$ , for major orders, is thus, plotted against the engine speeds.

The results for base engine roll, twist, and bend metrics are shown in the 'Results: Order-wise base engine roll, twist, and bend magnitude versus engine speed'.

## Results

In this section, the postprocessed measured vibration data and the postprocessed predicted vibration data are compared to each other using charts. As three postprocessing methods have been used, this section has been divided into three sub-sections, each sub-section corresponding to a different postprocessing method.

**Peak-hold acceleration magnitude versus frequency**

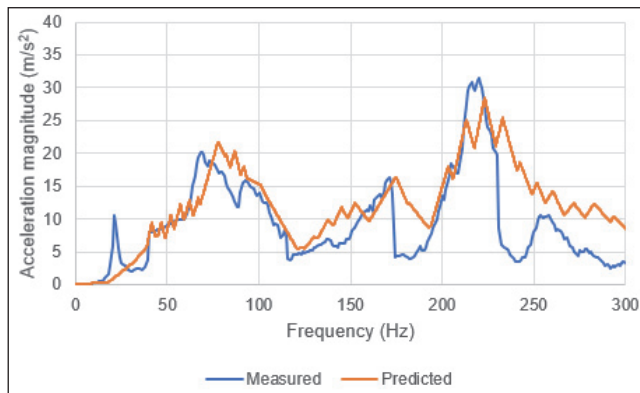


**Figure 6.** Peak-hold acceleration magnitude versus frequency chart for location 1 in lateral direction (x direction as shown in figures 2 and 3).

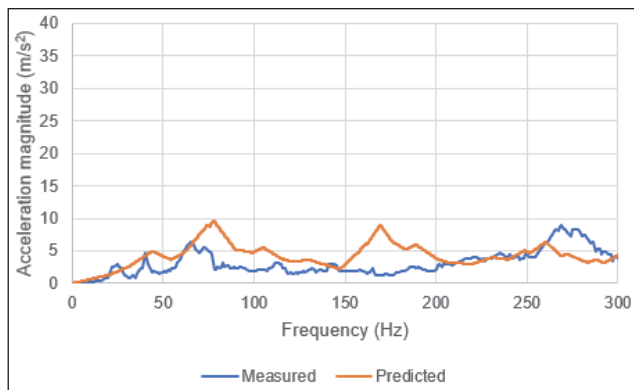


**Figure 7.** Peak-hold acceleration magnitude versus frequency chart for location 1 in vertical direction (y direction as shown in figures 2 and 3).

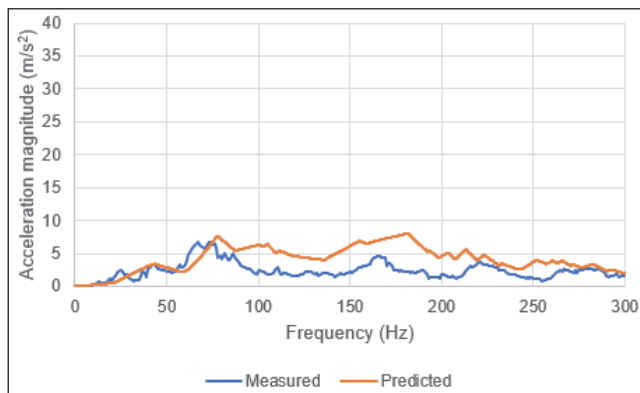


**Figure 8.** Peak-hold acceleration magnitude versus frequency chart for location 1 in axial direction (z direction as shown in figures 2 and 3).

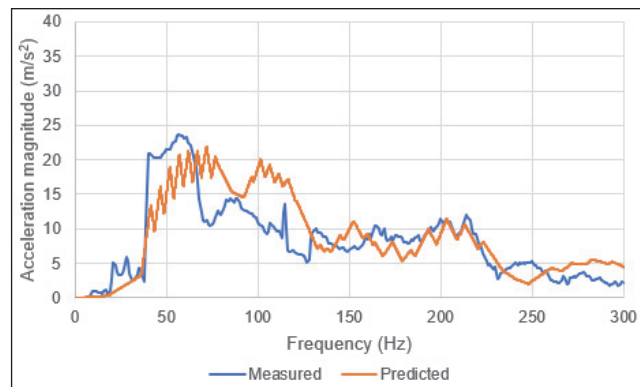


**Figure 9.** Peak-hold acceleration magnitude versus frequency chart for location 2 in lateral direction (x direction as shown in figures 2 and 3).

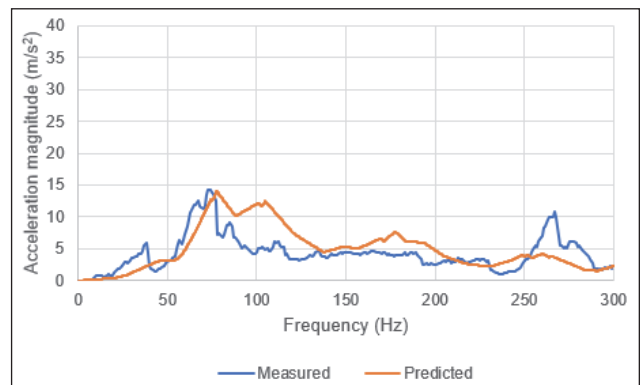


**Figure 10.** Peak-hold acceleration magnitude versus frequency chart for location 2 in vertical direction (y direction as shown in figures 2 and 3).

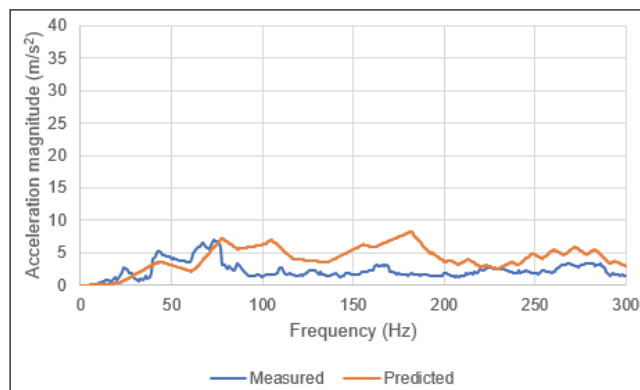


**Figure 11.** Peak-hold acceleration magnitude versus frequency chart for location 2 in axial direction (z direction as shown in figures 2 and 3).

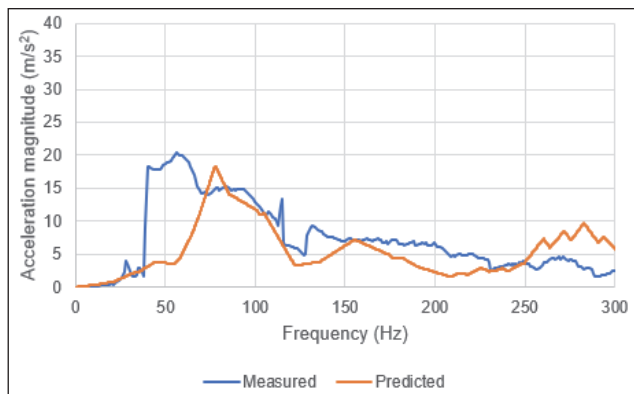


**Figure 12.** Peak-hold acceleration magnitude versus frequency chart for location 3 in lateral direction (x direction as shown in figures 2 and 3).

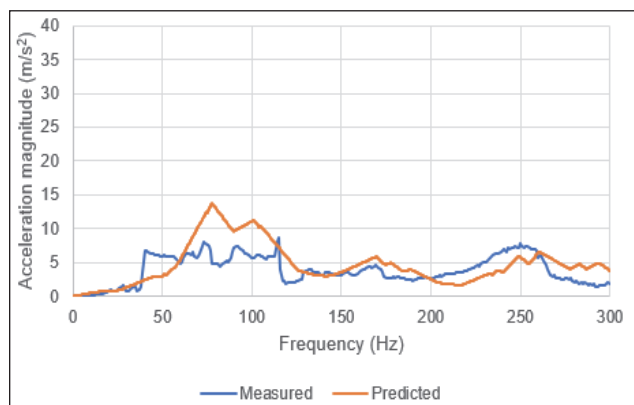


**Figure 13.** Peak-hold acceleration magnitude versus frequency chart for location 3 in vertical direction (y direction as shown in figures 2 and 3).

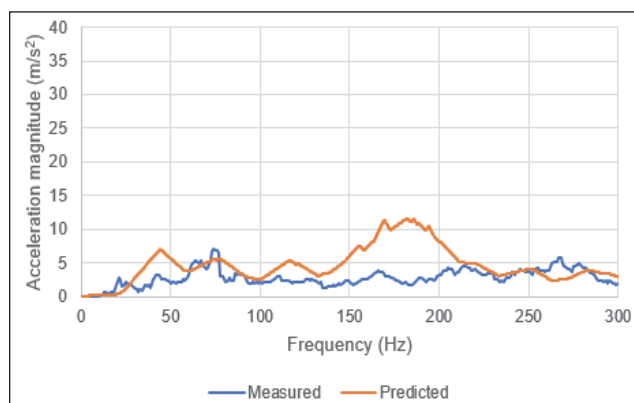


**Figure 14.** Peak-hold acceleration magnitude versus frequency chart for location 3 in axial direction (z direction as shown in figures 2 and 3).

### Order-wise acceleration magnitude versus engine speed

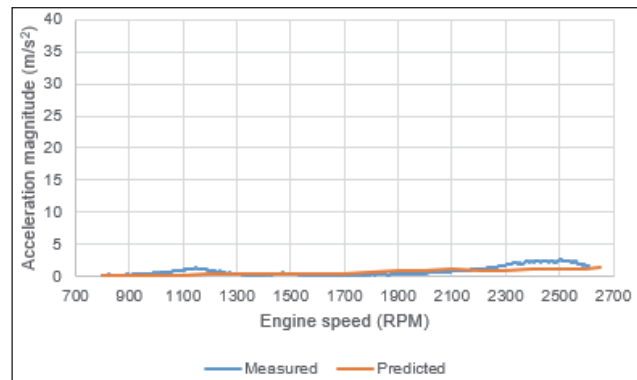


**Figure 15.** Order-wise acceleration magnitude versus engine speed chart for location 3: 1.5 order response in lateral direction (x direction as shown in figures 2 and 3).

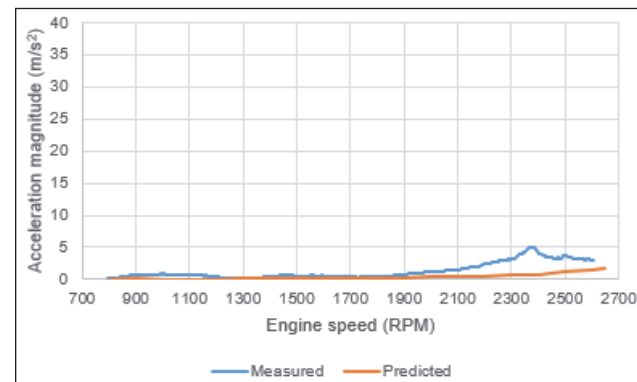


**Figure 16.** Order-wise acceleration magnitude versus engine speed chart for location 3: 1.5 order response in vertical direction (y direction as shown in figures 2 and 3).

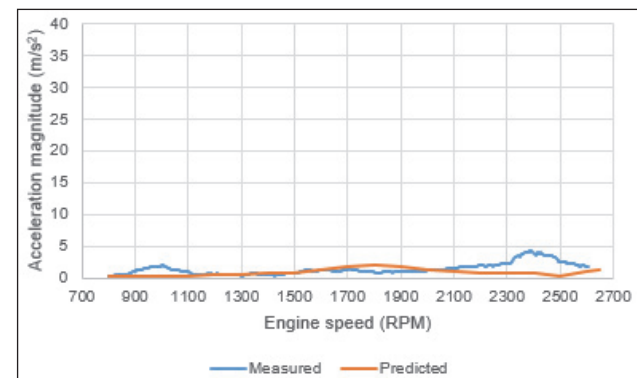


**Figure 17.** Order-wise acceleration magnitude versus engine speed chart for location 3: 1.5 order response in axial direction (z direction as shown in figures 2 and 3).

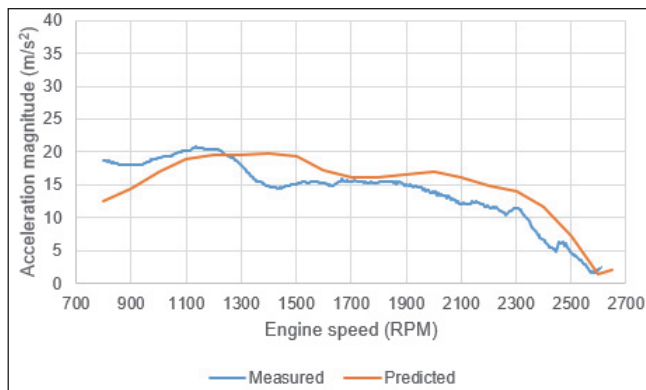


**Figure 18.** Order-wise acceleration magnitude versus engine speed chart for location 3: 3 order response in lateral direction (x direction as shown in figures 2 and 3).

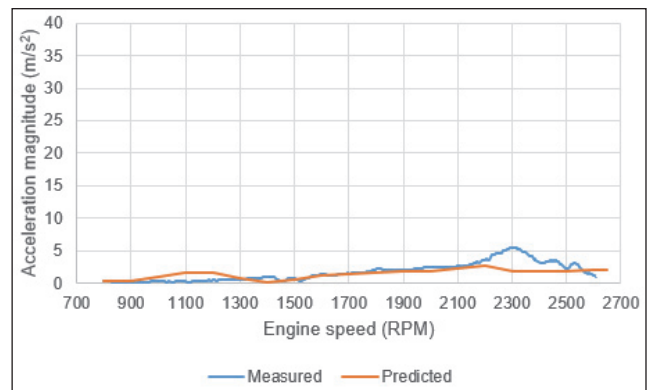


**Figure 21.** Order-wise acceleration magnitude versus engine speed chart for location 3: 4.5 order response in lateral direction (x direction as shown in figures 2 and 3).

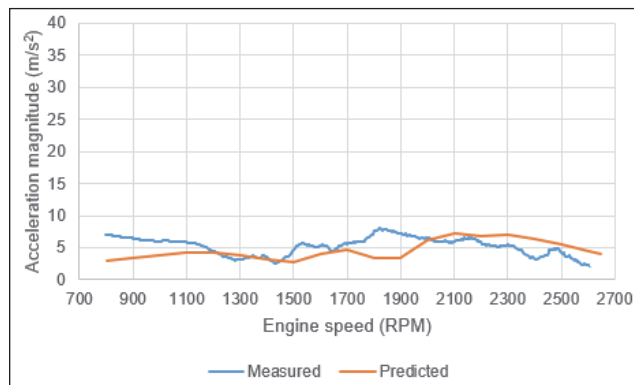


**Figure 19.** Order-wise acceleration magnitude versus engine speed chart for location 3: 3 order response in vertical direction (y direction as shown in figures 2 and 3).

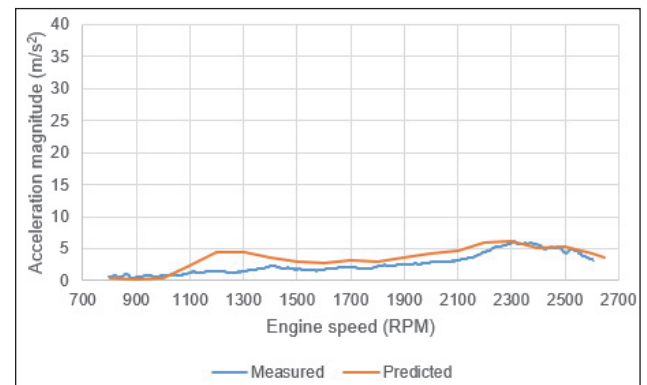


**Figure 22.** Order-wise acceleration magnitude versus engine speed chart for location 3: 4.5 order response in vertical direction (y direction as shown in figures 2 and 3).

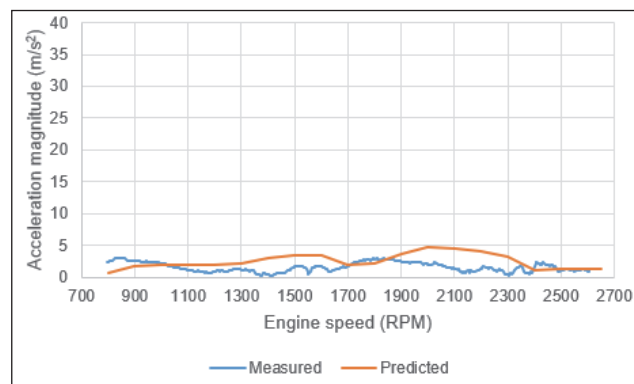


**Figure 20.** Order-wise acceleration magnitude versus engine speed chart for location 3: 3 order response in axial direction (z direction as shown in figures 2 and 3).

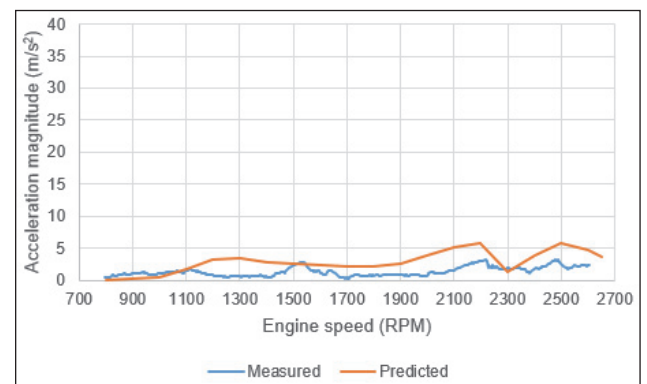


**Figure 23.** Order-wise acceleration magnitude versus engine speed chart for location 3: 4.5 order response in axial direction (z direction as shown in figures 2 and 3).

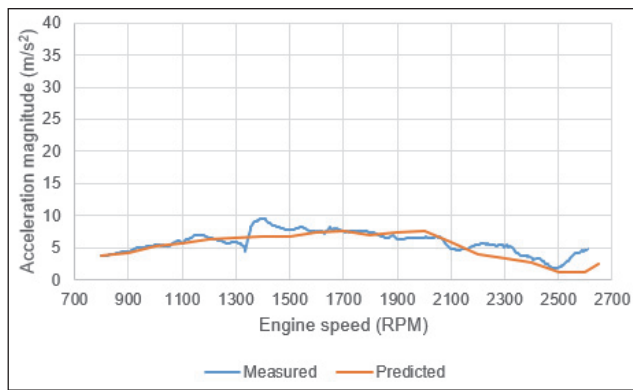


**Figure 24.** Order-wise acceleration magnitude versus engine speed chart for location 3: 6 order response in lateral direction (x direction as shown in figures 2 and 3).

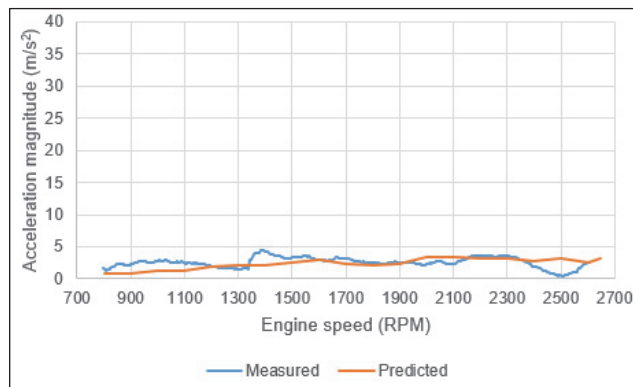


**Figure 25.** Order-wise acceleration magnitude versus engine speed chart for location 3: 6 order response in vertical direction (y direction as shown in figures 2 and 3).

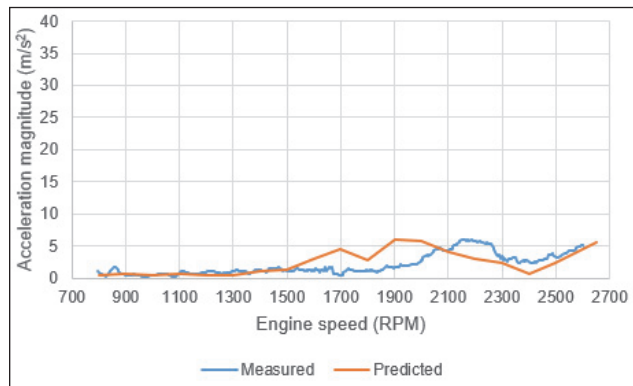


**Figure 26.** Order-wise acceleration magnitude versus engine speed chart for location 3: 6 order response in axial direction (z direction as shown in figures 2 and 3).

**Order-wise base engine roll, twist, and bend magnitude versus engine speed**

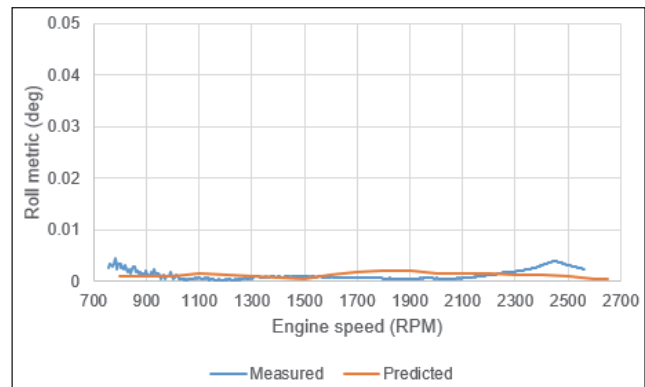


**Figure 27.** Order-wise base engine roll magnitude versus engine speed chart: 1.5 order response.

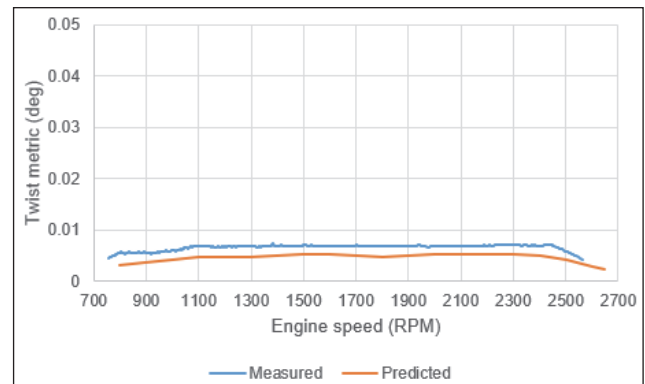


**Figure 28.** Order-wise base engine twist magnitude versus engine speed chart: 1.5 order response.

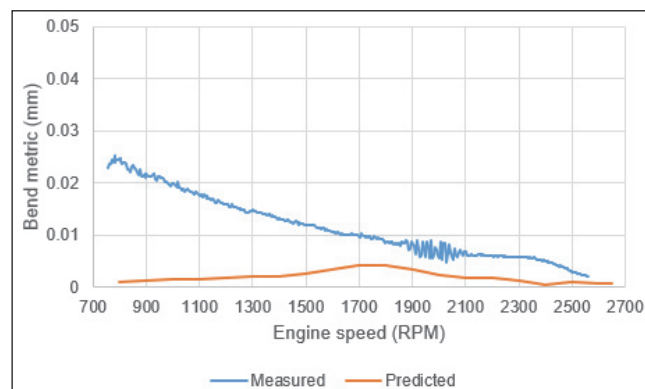


**Figure 29.** Order-wise base engine bend magnitude versus engine speed chart: 1.5 order response.

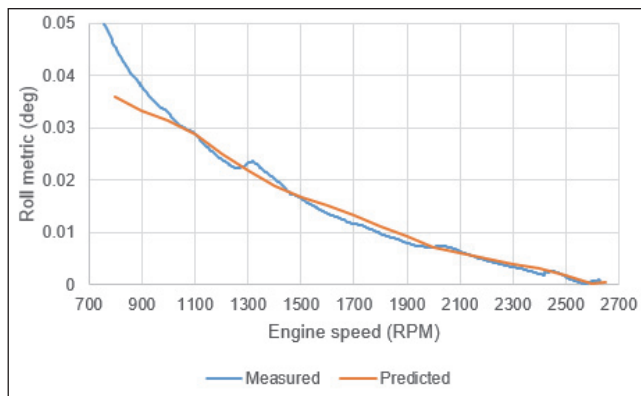


**Figure 30.** Order-wise base engine roll magnitude versus engine speed chart: 3 order response.

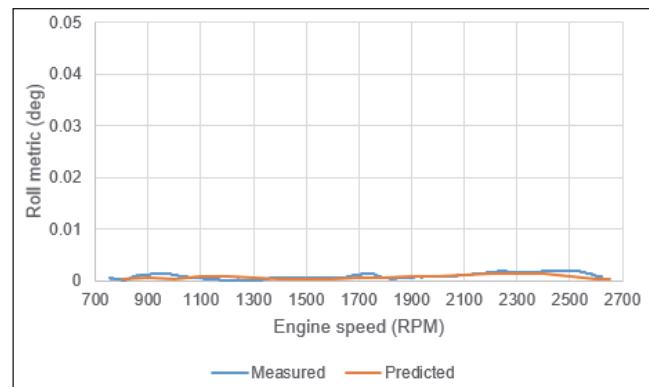


**Figure 33.** Order-wise base engine roll magnitude versus engine speed chart: 4.5 order response.

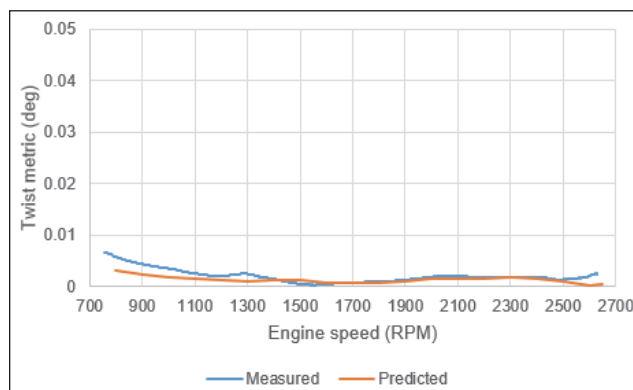


**Figure 31.** Order-wise base engine twist magnitude versus engine speed chart: 3 order response

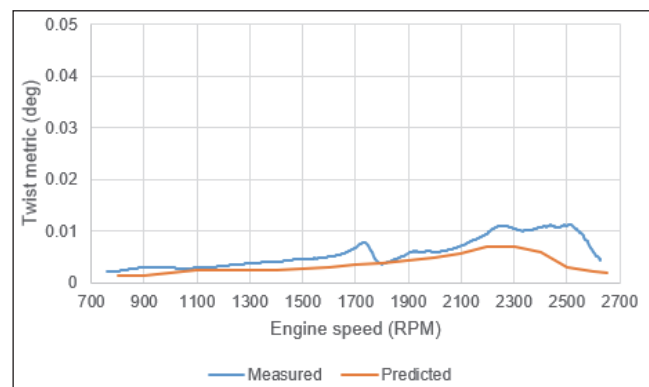


**Figure 34.** Order-wise base engine twist magnitude versus engine speed chart: 4.5 order response

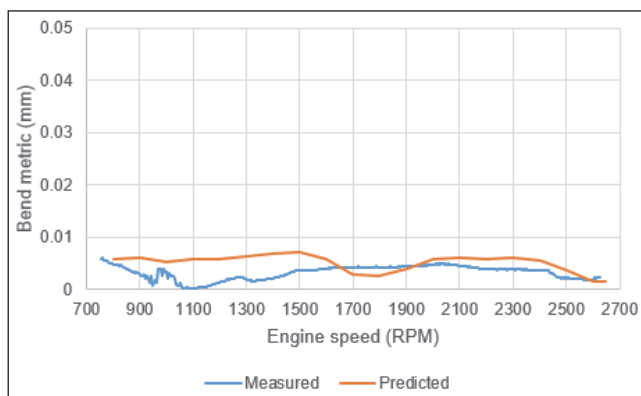


**Figure 32.** Order-wise base engine bend magnitude versus engine speed chart: 3 order response

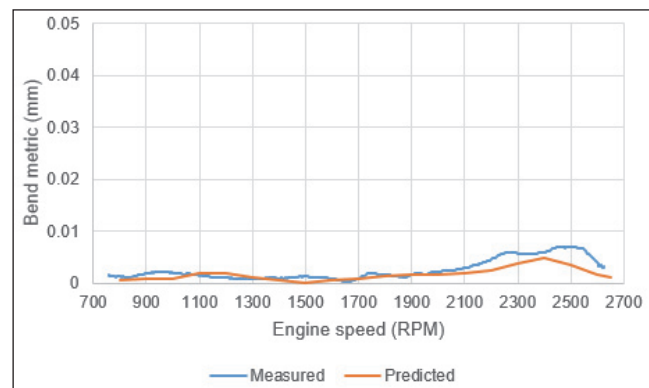


**Figure 35.** Order-wise base engine bend magnitude versus engine speed chart: 4.5 order response.

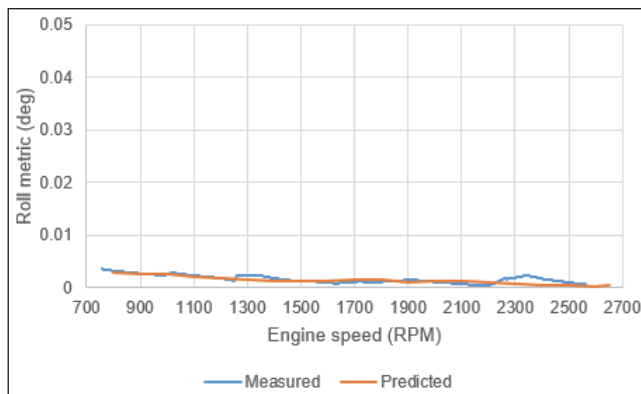


**Figure 36.** Order-wise base engine roll magnitude versus engine speed chart: 6 order response.

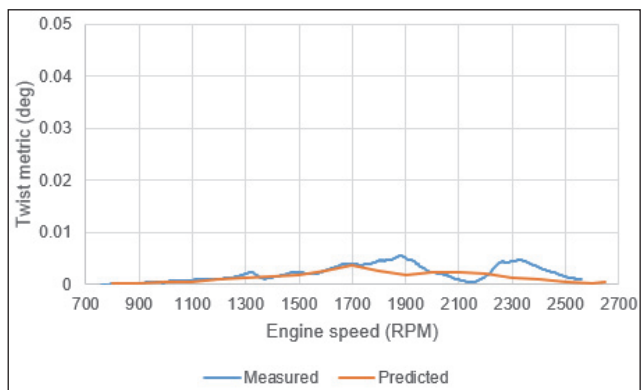


**Figure 37.** Order-wise base engine twist magnitude versus engine speed chart: 6 order response.

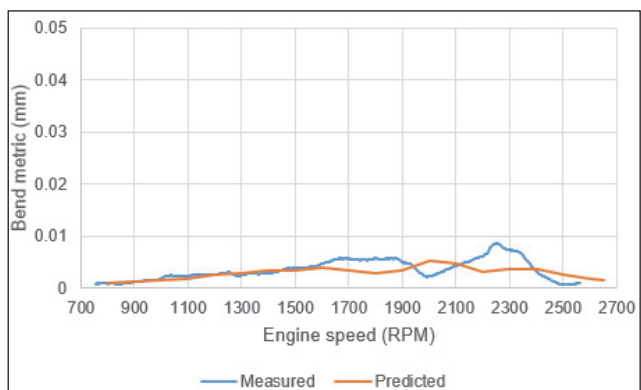


**Figure 38.** Order-wise base engine bend magnitude versus engine speed chart: 6 order response.

### Discussion

A discussion on the results displayed in the 'Results' section follows.

### Peak-hold acceleration magnitude versus frequency

In location 1 lateral direction measured data, there are three prominent peaks in acceleration magnitude. These peaks are close to 70 Hz, 170 Hz, and 220 Hz. These three peaks are captured by simulation as well.

In location 2 lateral direction measured data, there are two prominent peaks in acceleration magnitude. These peaks are close to 60 Hz and 210 Hz. Simulation too, shows peaks close to these frequencies. However, simulation also shows a third peak close to 100 Hz, that is not found in measured data.

In location 3 lateral direction measured data, there is one prominent peak in acceleration magnitude. This peak is at 60 Hz. In simulation, the frequency of this peak is over-predicted to be close to 75 Hz. Further, there is an additional peak in predicted acceleration magnitude, close to 270 Hz, that is not found in measured data.

For the vertical and axial directions, the measured acceleration magnitude does not exceed  $15 \text{ m/s}^2$ , across the spectrum. This is true for all the three locations on the base engine. A similar observation is made even for predicted acceleration magnitude.

### Order-wise acceleration magnitude versus engine speed

For 1.5 order response, both the measured and predicted data show an acceleration magnitude less than  $5 \text{ m/s}^2$ , for all the three directions. This is partly because 1.5 order excitation attempts to twist the base engine, and based on previous experience, there is no twist mode of the base engine under consideration, that is below 70 Hz, which is the 1.5 order's frequency corresponding to the highest engine speed under consideration.

The third order acceleration magnitude for lateral direction shows two prominent peaks in measured data. These peaks are at 1200 RPM (60 Hz) and 1800 RPM (90 Hz). Simulation predicts these peaks as having similar acceleration magnitudes as measured data but both the peaks are offset by 200 RPM (10 Hz). Both

measurement and simulation predict the third order acceleration magnitude to be below  $10 \text{ m/s}^2$  for vertical and axial directions.

Both measurement and simulation predict a 4.5 order acceleration magnitude response to be below  $10 \text{ m/s}^2$  for all the three directions.

Simulation is able to predict the sixth order lateral acceleration magnitude close to the measured data for almost the entire engine speed range. The sixth order vertical acceleration magnitude is below  $5 \text{ m/s}^2$ , both in measurement and prediction. In the axial direction, the engine speed at which the predicted acceleration magnitude peaks, is about 300 RPM (30 Hz) lower than that found in measured data.

#### **Order-wise base engine roll, twist, and bend magnitude versus engine speed**

Both the measured and predicted data show the 1.5 order roll metric as not exceeding 0.005 deg for the entire speed range. Simulation predicts a 1.5 order twist amplitude that is consistently lower as compared to the measured data. This may indicate a higher engine twist stiffness in simulation as compared to testing. The predicted 1.5 order bend response shows a trend that is significantly different as compared to the measured data.

The third order predicted roll response matches very well with the measured data. The predicted twist metric for third order also matches fairly well with the measured data. The predicted bend metric for third order does not match well with the measured data, but both predicted and measured data show a maximum bend metric value below 0.01 mm, for the entire engine speed range.

The 4.5 order roll and bend metrics, show a close match between predicted and measured data, for most of the engine speed range. The 4.5 order twist metric shows a peak close to 1750 RPM (131 Hz) in measured data, which is over-predicted to be at 2250 RPM (169 Hz). This, just like the observation in 1.5 order twist, may possibly be due to higher twist stiffness of base engine in simulation as compared to testing.

Both simulation and measurement show a sixth order roll metric to be below 0.005 deg. This is

partly due to absence of any mount roll mode in the frequency range from 70 Hz (700 RPM) to 270 Hz (2700 RPM). As in the case of 4.5 order twist metric, the mode of 131 Hz (1310 RPM) is being predicted to be at 169 Hz (1690 RPM), possibly due to higher engine twist stiffness in simulation as compared to testing. The sixth order bend response is below 0.01 mm for both simulation and testing, for the entire engine speed range.

#### **Conclusions**

After using the three postprocessing methods, it may be concluded that, even though there is a good match between measured vibratory response and predicted vibratory response on the base engine for a few locations, orders, and metrics, there is a significant scope for improvement in this correlation, in an overall sense.

A crucial step towards improving this correlation is to reduce the uncertainty in the inputs which are mentioned in the 'Modeling of the engine: Uncertainty in inputs' section. This would firstly, imply use of instantaneous cylinder pressure data from the same test, from which the vibratory response data is extracted. Secondly, the rotating assembly that is attached to the rear of the flywheel, could be modeled with accurate information about its mass and geometry. Thirdly, the vibration isolators that are used to connect the condensed stationary model to the ground, could be modeled using a measured dynamic stiffness along each of the three Cartesian directions.

#### **Conflict of Interest and Funding**

The authors would like to state that there is no conflict of interest involved in the presented work.

Further, the authors acknowledge that the source of funding of all the testing and simulation, necessary for the presented work is Cummins Inc.

#### **Acknowledgments**

The authors would like to thank Neha A Patil and Deepa Patil from Cummins Technical Centre India, for providing some of the inputs necessary for simulation.

### References

- [1] Meirovitch, L. and Parker, R.G., Fundamentals of vibrations, *Appl. Mech. Rev.*, 2001, 54(6): B100-B101. <https://doi.org/10.1115/1.1421112>
- [2] Seshu, P., Substructuring and component mode synthesis, *Shock and Vibration*, 1997, 4(3): 199-210. <https://doi.org/10.1155/1997/147513>
- [3] Craig Jr, R.R. and Bampton, M.C., Coupling of substructures for dynamic analyses, *AIAA journal*, 1968, 6(7): 1313-1319. <https://doi.org/10.2514/3.4741>
- [4] Wilson, W.K. *Practical solution of torsional vibration problems: with examples from marine, electrical, aeronautical, and automobile engineering practice*, 1956, Vol. 2, Springer, New York, NY, USA.
- [5] Nestorides, E.J., *A handbook on torsional vibration*, 1958, Cambridge University Press, Cambridge, United Kingdom.
- [6] Den Hartog, J., *Mechanical Vibrations*, 1956, McGraw-Hill, New York, NY, USA.
- [7] Richards, C.M. and Singh, R., Characterization of rubber isolator nonlinearities in the context of single-and multi-degree-of-freedom experimental systems, *Journal of Sound and vibration*, 2001, 247(5): 807-834. <https://doi.org/10.1006/jsvi.2001.3759>
- [8] Bracewell, R.N. *The Fourier transform and its applications*, 1986, Vol. 31999, McGraw-Hill, New York, NY, USA.
- [9] Bracewell, R.N., The fourier transform, *Scientific American*, 1989, 260(6): 86-95. <https://doi.org/10.1038/scientificamerican0689-86>
- [10] Røhndal, P. and Nielsen, H.B., Firing Order Selection in Relation to Vibration Aspects, *Proceedings of Internal Combustion Engine Division Spring Technical Conference, Salzburg, Austria*, 2003, 36789: 311-320. <https://doi.org/10.1115/ices2003-0603>
- [11] Uicker, J.J., Pennock, G.R., Shigley, J.E. and McCarthy, J.M., *Theory of machines and mechanisms*, 2003, Vol. 768, Oxford University Press. New York, NY, USA. <https://doi.org/10.1115/1.1605769>